Carbohydrate Research 354 (2012) 21–31

Contents lists available at SciVerse ScienceDirect

Carbohydrate Research

journal homepage: www.elsevier.com/locate/carres

Synthesis and characterization of a paramagnetic sialic acid conjugate as probe for magnetic resonance applications

Davide Bini [a], Maria Gregori [b,†], Ugo Cosentino [c], Giorgio Moro [a], Angeles Canales [e], Alice Capitoli [a], Jesús Jiménez-Barbero [a,d], Laura Cipolla [a,*]

[a] Department of Biotechnology and Biosciences, University of Milano-Bicocca, Piazza della Scienza 2, 20126 Milano, Italy
[b] Department of Experimental Medicine, University of Milano-Bicocca, via Cadore 48, 20052 Monza, Italy
[c] Department of Environmental Sciences, University of Milano-Bicocca, Piazza della Scienza 1, 20126 Milano, Italy
[d] Centro de Investigaciones Biológicas, CSIC, Ramiro de Maeztu 9, 28040 Madrid, Spain
[e] Dep. Química Orgánica I, Facultad Ciencias Químicas, Universidad Complutense de Madrid, Avenida Complutense s/n, 28040 Madrid, Spain

ARTICLE INFO

Article history:
Received 13 January 2012
Received in revised form 29 February 2012
Accepted 3 March 2012
Available online 17 March 2012

Keywords:
Sialic acid
Molecular modelling
Magnetic Resonance Imaging
Paramagnetic Relaxation Enhancement

ABSTRACT

Magnetic Resonance Imaging (MRI) using paramagnetic systems as contrast agents is receiving increased attention as diagnostic tool in the clinic. At the same time, NMR of paramagnetic systems can also be applied in biochemical fields; for example, the use of Paramagnetic Relaxation Enhancement (PRE) allows structure refinement and the analysis of transient dynamic processes involved in macromolecular complex formation. Herein we report the synthesis and computational characterization of a new DOTA-like sialic acid conjugate, which can be used both in MRI and PRE applications when coordinated to a suitable paramagnetic metal.

1. Introduction

N-Acetylneuraminic acid (Fig. 1, NeuAc, **1**) represents the most ubiquitous member of the sialic acid family of derivatives found on cell surface glycoproteins and glycolipids.[1] It plays important roles in many physiological and pathological processes[2] such as regulation of biofluid and mucin viscosity,[3] and disaggregation of cells by repulsive effects.[4] Moreover, as terminal substituents, sialic acids are ideally suited to participate in protein–carbohydrate interactions that mediate cell surface recognition phenomena. Indeed, cell surface sialosides are known to serve as ligands for microbial toxins,[5,6] bacterial and viral adhesins,[7] and for mammalian lectins responsible for cell–cell adhesion.[8] In addition, aberrant glycosylation is known to be a common feature of cancer cells[9] and, in particular, alteration of sialic acids is thought to be a characteristic associated with malignant properties[10] including invasiveness and metastatic potential. Sialidases, which catalyses the removal of sialic acid residues from glycoproteins and glycolipids, have also been suggested to play important roles in many biological processes through regulation of sialic acid contents in glycoconjugates.[11] Altered expression of sialidase has been observed in cancer, therefore suggesting its involvement in the malignant process. These results indicate that high expression of sialidase in cancer cells leads to protection against programmed cell death, probably by modulation of gangliosides.[12] It has been shown that levels of mRNA of human plasma membrane-associated sialidase (Neu3) are increased in human colon cancer by 3- to 100-fold compared to adjacent non-tumour mucosa.[13] These findings highlight Neu3 as a potential target for diagnosis and therapy of certain type of cancers.

Nuclear magnetic resonance (NMR) techniques involving paramagnetic systems are today valuable tools that can find applications in relevant fields, such as Magnetic Resonance Imaging (MRI), and in biochemical issues[14] with the use of Paramagnetic Relaxation Enhancement (PRE). Among different diagnostic techniques, Magnetic Resonance Imaging (MRI)[15] using paramagnetic systems as contrast agents is receiving increased attention because it is non-invasive and provides information about biological structure and function of whole organisms over time.[16,17]

Due to the electronic properties of the gadolinium ion, Gd(III) complexes are currently employed in clinical practice as contrast agents in MRI techniques.[14,15] Contrast agents improve the contrast in images by enhancing the nuclear magnetic relaxation rates of the water protons in the tissues where they are distributed. The mechanism of relaxation enhancement, that is, relaxivity, involves dipolar interactions between the magnetic moment of the metal

* Corresponding author. Tel.: +39 02 64482152; fax: +39 02 64483565.
E-mail address: laura.cipolla@unimib.it (L. Cipolla).
† Present address.

0008-6215/$ - see front matter © 2012 Elsevier Ltd. All rights reserved.
http://dx.doi.org/10.1016/j.carres.2012.03.002

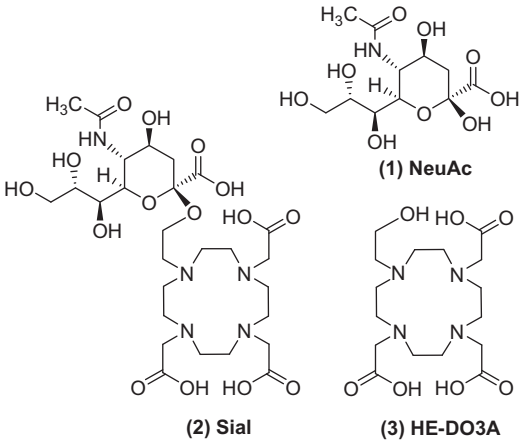

Figure 1. Molecular structures of neuraminic acid (NeuAc, **1**), the sialic acid conjugate Sial (**2**) and of HE-DO3A (**3**).

ion and the nuclear spin of the water protons. Octadentate polyamino carboxylate ligands (PAC) such as DOTA (DOTA = 1,4,7,10-tetrakis(carboxymethyl)-1,4,7,10-tetraaza-cyclododecane), form kinetically and thermodynamically stable complexes with gadolinium: the ninth coordination site of Gd allows rapidly exchanging water molecules to transmit the paramagnetic relaxation effect to the bulk solvent. Today, the search for new Gd-based contrast agents is oriented toward developing compounds that possess binding ability toward specific biological targets.[15] By conjugating a suitable targeting vector to the metal chelate it may be possible to target tissue type, cell type, individual proteins and even specific nucleic acid sequences. Among the different targeting strategies, there is an approach proposed for constructing 'conditional' MRI contrast agents, that is, contrast agents that switch states between low-relaxivity (inactive) and high-relaxivity (active) by the action of a specific enzyme.[18]

On the other hand, relevant advances have been achieved in the use of PRE in structure refinement and in the analysis of transient dynamic processes involved in macromolecular complex formation.[19] The PRE technique is based on magnetic dipolar interactions between a nucleus (e.g., ^{1}H) and the unpaired electrons of a paramagnetic centre, and results in an increase in the relaxation rate of the nuclear magnetization.[20] For a given electron–nucleus distance r, the magnitude of the PRE is proportional to r^{-6}, a relationship analogous to that between the magnitude of the NOE and interproton distance. However, because the magnetic moment of the unpaired electron is large, the PRE effects are large and can provide long-range distance information, extending in the case of Mn^{2+}, for example, up to ≈35 Å. Recent applications include for example rapid elucidation of protein–protein,[21] and protein–oligosaccharide interactions and mapping of binding sites.[22] Independently from the magnetic resonance technique of choice, the system necessitates the attachment of an extrinsic paramagnetic group to the (macro)molecule of interest through appropriate chemical modification.

To date only a few examples have been focused on paramagnetic sialic acid conjugates, and on detection of sialic acids,[23] while several examples of targeted MRI contrast agents toward other glycan structures have been reported.[24] Herein we report the synthesis of a new DOTA-like sialic acid conjugate, named Sial (**2**, Fig. 1), which can be used both in MRI and PRE applications, when coordinated to a suitable paramagnetic metal. The sialic acid conjugate **2** consists of the HE-DO3A ligand (HE-DO3A = 10-(2-hydroxyethyl)-1,4,7,10-tetraazacyclododecane 1,4,7-tetraacetate, **3**, Fig. 1) covalently α-linked to a sialic acid moiety via the hydroxyethyl moiety.

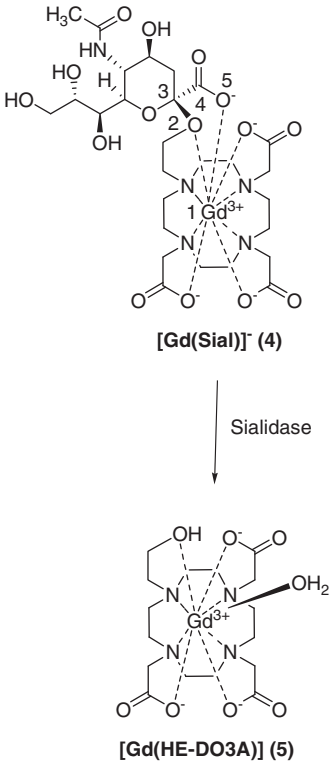

Figure 2. Structure of $[Gd(Sial)]^-$ (**4**) and proposed activation mechanism (including atomic numbering defining the τ torsion).

The conjugate **2**, when complexed to a suitable paramagnetic metal such as gadolinium ($[Gd(Sial)]^-$, **4**, Fig. 2) can be used as a conditional MRI contrast agent, relying on the hypothesis that selective activation of the contrast agent in the tumour sites overexpressing Neu3 will occur. The approach capitalizes on the modulation relaxation rate that can be achieved by altering the hydration number (q) of the contrast agent, as reported in the literature on analogous examples.[18,25] Before the cleavage, the sugar moiety should prevent the contrast agent activity, hindering coordination of a water molecule to the ninth coordination site of the gadolinium ion (q = 0). In the presence of sialidases, the neuraminic acid should be cleaved from the chelate allowing coordination of a water molecule (q = 1) and restoring the contrast agent activity (Fig. 2). Hence, exploiting differences in sialidase expression and activity in cancer areas, complex **4** would be cleaved by endogenous overexpressed sialidases. This hypothesis is supported by the fact that several glycosidases have been reported to cleave other DOTA-monosaccharide conjugates.[25,26]

The same sialic acid conjugate **2** can find applications also in PRE techniques when complexed to different paramagnetic metals. NMR spectra may usually be obtained from complexes of paramagnetic lanthanide ions with organic ligands.[27] Such spectra commonly show paramagnetic shifts, mainly of dipolar (pseudocontact) origin, of between 0 and 20 ppm, which are approximately proportional to $1/r^3$ (r = Ln–H distance). Large low-field shifts can be produced in the receptor spectrum, and hence yield structural information in addition to simplifying the spectrum itself. Moreover, NMR of lanthanide derivatives helps in capturing long time scale motions. As highlighted previously, sialic acids are typically found at the non-reducing termini of many glycan chains where it is responsible for carbohydrate mediated intercellular and intracellular events. A suitable paramagnetic neuraminic acid complex might help in deciphering relevant ligand/receptor interactions occurring in recognition phenomena involving sialic acids.[28]

2. Results and discussion

To evaluate if the designed sialic acid complex **4** could be a promising candidate for MRI applications, we investigated the possible conformational equilibria by computational methods.

2.1. Computational studies on $[Gd(Sial)]^-$

Conformational equilibria in aqueous solution of $[Gd(Sial)]^-$ have been investigated by ab initio calculations and classical MD simulations. Solvent effects have been included in the ab initio calculations by means of a continuum approach,[29] the polarizable continuum model (PCM),[30] and in MD simulations by explicit water molecules. MD simulations of the $[Gd(Sial)]^-$ system were performed describing interactions of the gadolinium ion with the eight donor atoms of the PAC ligand by a valence force field, while interactions at the ninth-coordination site of the gadolinium ion that involve water molecules, or other donor atoms of the sialic residue, are modelled by non bonded (electrostatic and van der Waals) potential. Force field parameters for gadolinium–ligand interactions were those previously developed.[31]

Preliminary Molecular Mechanics calculations (see Computational Methods) showed that the (A+) and (A−) diastereoisomeric conformations present similar energies, lower than those of B(+) and (B−) (see Computational Methods for IUPAC nomenclature of the four conformations). The (A+) conformation was slightly more stable and thus was selected for successive investigation. The most relevant conformational degree of freedom in $[Gd(Sial)]^-$ is the τ torsion (Gd_1–O_2–C_3–C_4 in Fig. 2), defining the relative orientation of the sialic acid moiety with respect to the coordination cage. Three starting conformations, differing in the orientation of the sialic acid, were used as starting points for simulations, with τ value of 0°, 90°, and 180°.

Each conformation was submitted to MD simulations in aqueous solution. In the first and third runs the τ torsion presents on average values close to the starting ones, that is, −27° and 172°, respectively (Table 4); in the second run τ rapidly (within 40 ps) increases to a mean value close to that of the third run. Thus MD simulation indicates the presence of two stable conformations, here labelled as C_1 and C_2, in which the different orientations of the sialic moiety cause different coordination situations around the ion. In C_1, the ninth coordination position is stably occupied by one carboxylic oxygen of the sialic moiety, with an average Gd–O_5 distance of 2.26 Å, while in C_2, the ninth coordination position is stably occupied by one water molecule, even if one water exchange event occurred during the simulation period (20 ns). Figure 3 shows the radial distribution function (rdf) of the water oxygen atoms around the ion in the two conformations and Table 1 reports the distance of the first maximum in the rdf. In C_1, the maximum of the first peak appears at 3.93 Å, thus confirming that no water molecules coordinate the ion; in C_2, the first peak presents a maximum at 2.55 Å (peak integration provides a coordination number of 0.83), thus highlighting the quite stable coordination of one water molecule to the gadolinium ion.

Trajectory analysis (Table 1) shows that the torsions in the five-member rings involving gadolinium and acetate arms show only small fluctuations around the average values in the two conformations. On the other hand, the alcoholic arm adopts the same orientation of the acetate arms in C_1, while in C_2 it stably adopts an opposite orientation, although interconversions are here observed during the simulation (Table 1 and Fig. 4).

Average gadolinium–ligand bond distances (Table 1) compare well with experimental values in the analogue [Gd-HPDO3A] compound[32] (**HP-DO3A** = 10-(2-hydroxypropyl)-1,4,7,10-tetraazacyclododecane 1,4,7-tetraacetate): as already observed,[31] the Gd–O average MD bond distance values are well in line with experimental ones, while the Gd–N bond distances are slightly greater than the experimental values.

MD simulations show C_1 to be the most stable conformation, C_2 being 8.5 kcal mol^{-1} above C_1 (ΔE_{tot} in Table 2). Analysis of the energetic contributions shows that although the internal energy term (ΔE_{Sia}) favours C_2 over C_1, solvent interactions ($\Delta E_{Sia\text{-}wat}$) prevail in determining the overall C_1 stability.

To check the reliability of MD results, two representative snapshots from the C_1 and C_2 trajectories have been submitted to C-PCM ab initio geometry optimization. In both calculations, the presence of one water molecule is considered in the molecular system: in C_1 the water molecule is not coordinated to the ion and involved in hydrogen bond with the ligand, while it is coordinated to the ion in C_2.

The geometries of the C_1 and C_2 conformations of $[Gd(Sial)(H_2O)]^-$ calculated at the C-PCM HF/3-21G level are reported in Figure 5. C-PCM ab initio calculations and MD results provide essentially the same geometrical parameters (Table 1). Also the relative energies, calculated at the C-PCM PBE1PBE/6-311G** level, agree with MD results (Table 2): the C_1 conformation is the most stable one and the solvent interactions are decisive in determining the overall C_1 stability. In fact, analysis of the C-PCM

Table 1
Values of the main geometrical parameters (see Fig. 2 for atom numbering) of the investigated conformations of $[Gd(Sial)]^-$ from MD simulations and ab initio calculations

	$[Gd(Sial)]^-$ MD simulations		$[Gd(Sial)(H_2O)]^-$ C-PCM HF/3-21G		[Gd(HP-DO3A)] X-ray
	C_1	C_2	C_1	C_2	
Bond distances (Å)					
Gd–N	2.732 (.176)	2.743 (.191)	2.751 (.070)	2.741 (.016)	2.648 (0.007)
Gd–O	2.341 (.059)	2.327 (.073)	2.346 (.020)	2.337 (.011)	2.348 (0.035)
Gd–O_2	2.509 (.058)	2.491 (.058)	2.516	2.566	2.397
Gd–O_5	2.264 (.066)	—	2.378	—	—
Gd–O_{water}	3.93[a]	2.55[a]		2.460	2.507
Torsions (°)					
τ[b]	−27.1 (7.1)	172.3 (7.4)	−6.9	163.5	—
Acetate arm					
N–C–C–O	−31.0 (8.3)	−30.0 (7.9)	−29.4 (9.6)	−29.8 (11.5)	−23.5 (12.2)
Gd–N–C–C	41.1 (6.3)	40.6 (6.6)	37.5 (5.4)	37.6 (4.5)	34.1 (4.7)
Alcoholic arm					
N–C–C–O_2	−53.3 (6.5)	42.6 (22.1)	−59.0	61.3	−40.4
Gd–N–C–C	35.2 (9.2)	−9.3 (16.8)	45.6	−21.2	49.2

For comparison, values from the X-ray structure of [Gd(HP-DO3A)] are reported.[32] Standard deviations in parenthesis.
[a] Gd–O_{water} distance from the first maximum in the rdf of the water oxygen atoms around the ion.
[b] The τ torsion is defined by atoms: Gd_1–O_2–C_3–C_4 (see Fig. 2 for atomic numbering).

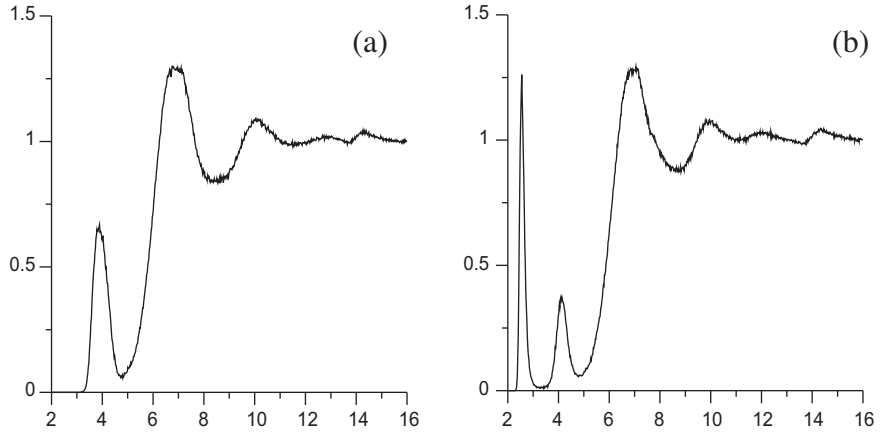

Figure 3. Radial distribution function of water oxygen atoms around the gadolinium ion in the (a) C_1 and (b) C_2 $[Gd(Sial)]^-$ conformations.

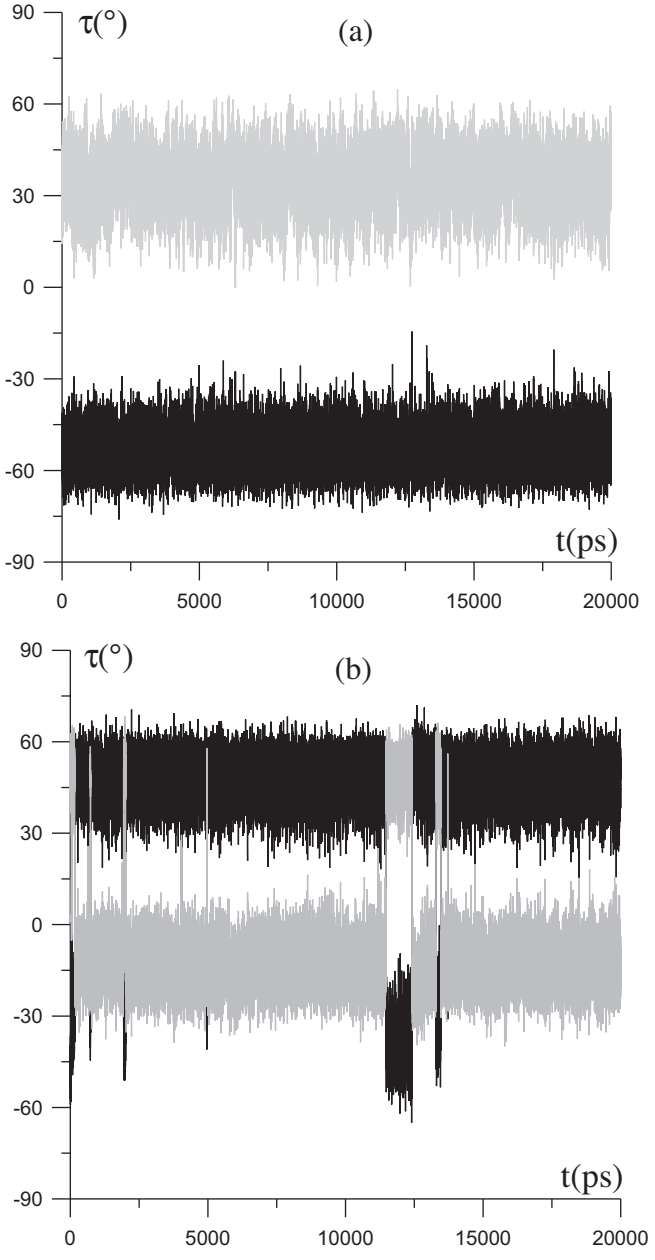

Figure 4. Alcoholic arm: trend of the N–C–C–O_2 (black) and Gd–N–C–C (grey) torsions along the trajectory in conformations (a) C_1, and (b) C_2.

Table 2
Relative energies (ΔE, kcal mol^{-1}) of C_2 conformation with respect to C_1, calculated from MD simulations and ab initio calculations[a]

	ΔE (C_2–C_1)
MD simulations[b]	
ΔE_{Sia}	−5.1 (10.0)
$\Delta E_{Sia\text{-}wat}$	13.5 (22.2)
$\Delta E_{\mathbf{Tot}}$	8.5 (24.3)
Ab initio calculations[c]	
ΔE°	−0.8
$\Delta\Delta G^{sol}$	6.4
ΔG^{tot}	5.6

Standard deviations from MD in parentheses.
[a] Absolute energy values are reported in Table 1S of the Supplementary data.
[b] ΔE_{Sia}, relative internal energy; $\Delta E_{Sia\text{-}wat}$, relative interaction energy with solvent water molecules; $\Delta E_{tot} = \Delta E_{Sia} + \Delta E_{Sia\text{-}wat}$, relative total energy.
[c] Calculations at the C-PCM PBE1PBE/6-311G** level on C-PCM HF/3-21G optimized geometries of $[Gd(Sial)(H_2O)]^-$. ΔE°, in vacuo relative total energies; $\Delta\Delta G^{sol}$, relative solvation free energies; $\Delta G^{tot} = \Delta E^\circ + \Delta\Delta G^{sol}$, relative total free energies in solution.

energetic contributions shows that in vacuo (ΔE° values) C_2 is more stable than C_1, while solvent interactions ($\Delta\Delta G^{sol}$ values) favour C_1.

The C_1 conformation, both in ab initio calculations and MD simulations, does not present a coordinated water molecule, that is, it is a 'closed' form corresponding to a low-relaxivity (MRI 'inactive') state. The C_2 conformation, significantly less stable than C_1, presents one coordinated water molecule and should represents an 'open' form corresponding to a high-relaxivity (MRI 'active') state. Thus, these results suggest that in the most stable conformation of $[Gd(Sial)]^-$, the gadolinium ion is not coordinated by a water molecule, and thus $[Gd(Sial)]^-$ can exist in an inactive form, able to switch to the active form by enzymatic cleavage.

2.2. Chemical synthesis

The retrosynthetic scheme for the synthesis of complex **4** is outlined in Scheme 1. In general, it should be noted that sialic acid manipulation is particularly challenging due to its complex chemical structure in comparison with other monosaccharides. Key steps are the glycosylation reaction, which requires stereochemical control toward the formation of the α-glycosidic linkage, naturally occurring in sialosides, and the DOTA monoalkylation reaction with 2′-bromoethyl α-sialoside.

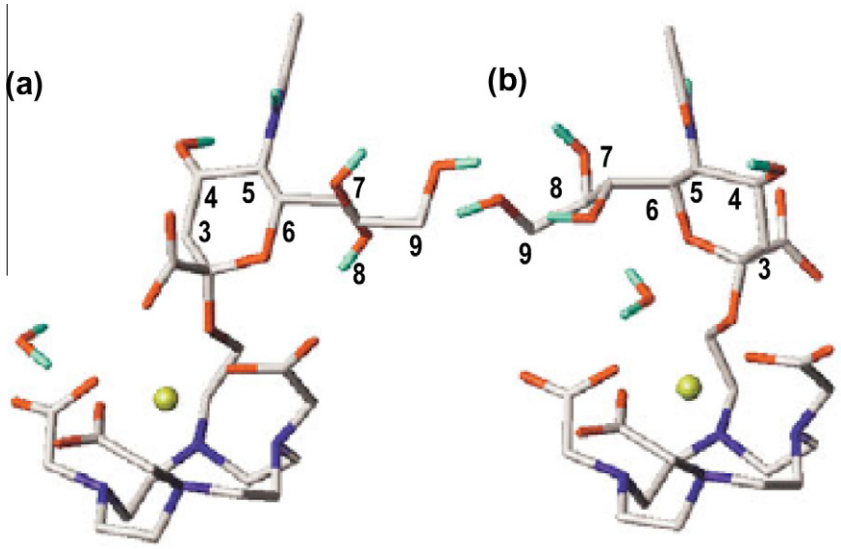

Figure 5. Molecular geometries of the (a) C_1 and (b) C_2 conformations of $[Gd(Sial)(H_2O)]^-$ calculated at the C-PCM HF/3-21G level.

First steps of the synthesis involve functional group protection according to literature procedure[33] (see Supplementary data for details).

To have access to the α-sialyl conjugate, glycosylation of a suitable sialyl donor with 2-bromoethanol in the presence of a promoter should be optimized toward α-stereoselection. The complicated molecular architecture of sialic acids imparts a substantial degree of difficulty in the glycosylation reaction. Even after appropriate protection, the presence of the anomeric carboxylic acid destabilizes the formation of the oxocarbenium ion intermediate through an inductive electron withdrawing effect. The steric constraints at the C-2 reactive site and the lack of an assistance from a neighbouring C-3 substituent often leads to low stereoselectivity and the formation of side-products through a competing elimination reaction.[34] In this context, we concentrated on the choice of the donor, the promoter and the solvent. The first glycosylation procedure that has been tried was a Koenigs–Knorr reaction[35] via the peracetylated β-sialyl chloride methyl ester (see Supplementary data for details).[36] However, sialyl chloride did not give the desired glycosylation product. Thus phenyl and tolyl thiosialosides were also tested as donors,[37] without any encouraging result. As a last attempt, peracetylated derivative **6**, was used as glycosyl donor, as already reported,[34b] in the presence of different Lewis acids as promoters (see Table 5S). The best conditions

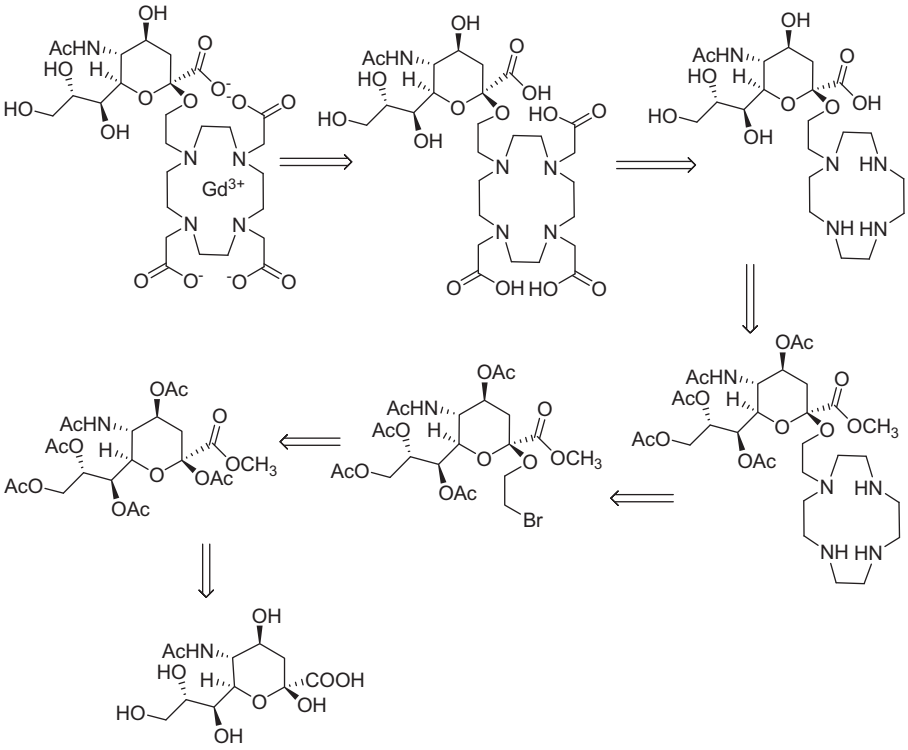

Scheme 1. Proposed retrosynthesis for $[Gd(Sial)]^-$.

use donor **6** and $BF_3{\cdot}OEt_2$ as the promoter and acetonitrile as the solvent (Table 5S and entry 13), as it is well known that it can help in affording α-anomeric glycosides through a kinetically controlled β-nitrilium ion intermediate.[38]

However, the low stereoselectivity (α/β ≈ 1:1) obtained in the previous conditions, prompted us to vary other parameters such as the promoter/acceptor molar ratio and the reaction time. First, an increase of the promoter/acceptor ratio from 1 to 5 caused a decrease in the α/β ratio. On the other hand, reduction of reaction time from 3 days to 3 h resulted in an increase in the α/to β ratio (Table 3).

An additional parameter was finally considered, after a recent publication which reports that a highly α-stereoselective sialylation (27:1 α/β) can be achieved by adding a non reactive compound, *N*-methyldiacetamide (DAMA) capable of modifying the supramolecular aggregation state of the glycosyl donor, thus influencing anomeric stereoselectivity.[39] Hence, the glycosylation reaction was also tried in the presence of DAMA, using different molar concentrations of the donor, as summarized in Table 4. However, we did not observe a significant increase in the stereoselection but unexpectedly observed a strong reduction in the formation of the competitive elimination product could be achieved. In summary, best conditions found to obtain the α-sialoside **7** are those reported in Table 4 (entry 2), which give 2:1 α/β ratio and 47% yields.

With the α-2′-bromoethylsialoside in hand we proceeded with the introduction of the HE-DO3A moiety, by alkylation of the suitably protected derivative **8** (Scheme 2). The reaction did not afford any product. Alternatively, different selective protection of three out of four nitrogen atoms of the cyclen was also attempted (BCl_3, $B(NMe_2)_3$, $POCl_3$),[40] but none of them afforded the desired product.

In a last attempt, we decided to try the conjugation between sialoside **7** and the unprotected cyclene moiety, by simply stirring compound **7** with cyclen overnight at rt.[25] Surprisingly, no polyalkylated by-products were observed (Scheme 3). The best solvent for the alkylation reaction was $CHCl_3$ both in terms of yield and reaction rate, among the several tried (dichloromethane, DMF, CCl_4, acetone and DMSO). Polyalkylation products were observed only when this reaction was performed at reflux temperature. The only by-product was the elimination product **2S** (see Scheme 1S).

Compound **10** was deacetylated under Zémplen conditions (Na, MeOH)[41] and the methyl ester hydrolysed with NaOH 1 M in H_2O.[42] Complete alkylation of **12** to yield **2** was achieved in 24 h by the addition of 3 equiv of bromoacetic acid in H_2O with K_2CO_3 as the base (Scheme 3). This reaction led also to the formation of trace amounts of incomplete alkylation of the cyclene moiety and of the esterification on the sialic acid's carboxylic group. Finally the paramagnetic metal was coordinated to the Sial (**2**) using $GdCl_3$ in H_2O.

2.3. NMR studies

1D proton NMR spectra were collected for the sialic acid conjugate Sial (**2**) in the presence of increasing amounts of Dy^{3+} (298 K, 600 MHz with cryoprobe). Addition of the paramagnetic ion gave rise to huge line broadening of all the proton signals of the molecule, even with a low amount of Dy^{3+}, at a molar ratio 2.5:1, sialic conjugate:metal (Fig. 6).

^1H–^{13}C HSQC spectra of 2 acquired at a molar ratio 2.5:1, sialic conjugate:Dy^{3+} (Fig. 7) displayed fewer signals than in the absence of the metal, because only 9-CH_2 and the acetamido CH_3 group

Table 3
Conditions for glycosylation reactions

Entry	Reagents	Ratio	Concn (M)	Time	*T*	Results
1	BF_3OEt_2–BrEtOH	0.05	0.12	3 days	rt	Degradation
2	BF_3OEt_2–BrEtOH	0.05	0.12	3 days	0 °C	Degradation
3	BF_3OEt_2–BrEtOH	0.5	0.12	3 days	0 °C	Degradation
4	BF_3OEt_2–BrEtOH	5	0.12	3 days	rt	Y = 33% (only β)
5	BF_3OEt_2–BrEtOH	5	0.12	5 h	rt	Y = 31% (α/β 1:1)
6	BF_3OEt_2–BrEtOH	1	0.12	3 h	rt	Y = 30% (α/β 2:1)

Table 4
Conditions for glycosylation reactions using DAMA

Entry	Reagents	Eq	Concn (M)	Time	*T*	Yield (α/β)
1	BF_3OEt_2–BrEtOH + DAMA	10/10/1	0.016	1 h + 3 h	rt	*Y* = 38% (1.5:1)
2	BF_3OEt_2–BrEtOH + DAMA	10/10/1	0.12	1 h + 3 h	rt	*Y* = 47% (2:1)

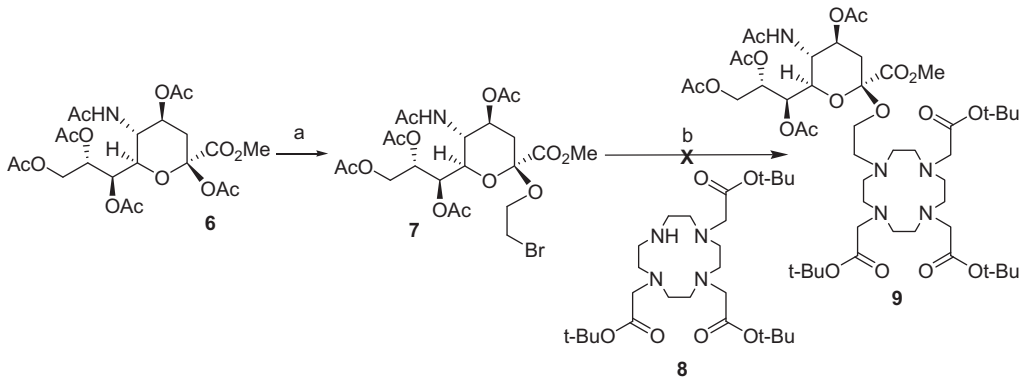

Scheme 2. Reagents and conditions: (a) BF_3OEt_2, BrEtOH, DAMA, CH_3CN; (b) **8**, $CHCl_3$, rt.

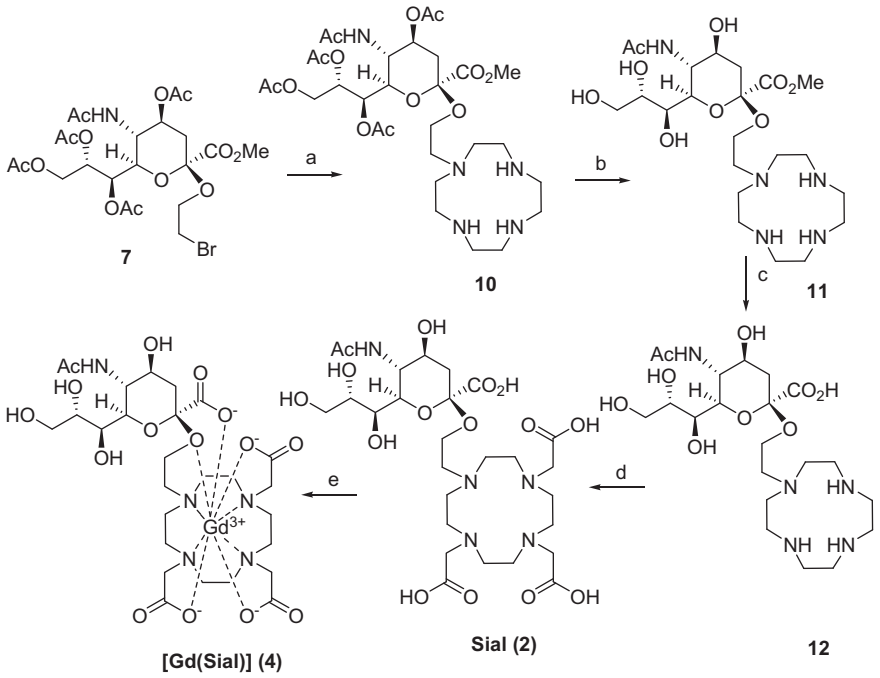

Scheme 3. Reagents and conditions: (a) cyclen, $CHCl_3$; (b) Na met., MeOH; (c) NaOH 1 M, H_2O; (d) $BrCH_2COOH$, K_2CO_3, H_2O; (e) $GdCl_3{\cdot}6H_2O$, H_2O.

could be detected. The loss of most of the signals could be due to the presence of complex mixtures of conformational isomers, as described by Grzesiek and co-workers[43] in other DOTA-like systems. In order to improve the quality, a new spectrum was recorded at a lower temperature (280 K) and at a higher sialic conjugate:metal ratio.

Acquisition of ^1H–^{13}C HSQC spectra of **2** at a 3.5:1 molar ratio and 280 K (600 MHz cryoprobe) allowed the detection of most of the sialic conjugate signals (Fig. 8). In these conditions, only CH-6 signal basically disappeared, while CH-7 significantly decreased its intensity. This is also in agreement with the presence of flexibility under these experimental conditions.

As the ionic radius of Dy^{3+} is somewhat smaller than that of Gd^{3+}, calculations have been also performed on the [Dy(Sial)$(H_2O)]^-$ system. The same C_1 and C_2 conformations have been found also in this case. Moreover, the relative total free energies in solution ΔG^{tot}, calculated at the C-PCM PBE1PBE/6-311G** level on C-PCM HF/3-21G optimized geometries, show that C_1 is the most stable conformation (ΔG^{tot} = 5.9 kcal mol^{-1}), as found for the Gd^{3+} system (ΔG^{tot} = 5.6 kcal mol^{-1}).

Comparison of the H/C–metal ion distances in the C_1 and C_2 conformations found in the computational analysis (Fig. 5) with the observed experimental NMR data did not allow a clear-cut non-ambiguous discrimination between the two conformations. Nevertheless in conformation C_2, the metal is rather close to the C3 protons and a decrease in the intensity of these hydrogens should be observed. Because no major changes in the intensity of these signals are observed in the corresponding HSQC, a low participation of this conformer should be expected.

3. Materials and methods

3.1. General

All solvents were dried over molecular sieves, for at least 24 h prior to use. When dry conditions were required, the reaction was performed under Ar atmosphere. Thin-layer chromatography (TLC) was performed on Silica Gel 60 F254 plates (Merck). The detection was performed with a solution containing concentrated H_2SO_4–EtOH–H_2O in a ratio of 5:45:45. Flash column chromatography was performed on silica gel 230–400 mesh (Merck). NMR spectra were recorded at 400 MHz (^1H) and at 100.57 MHz (^{13}C) on a Varian Mercury instrument or at 600 MHz (^1H) and at 150.91 MHz (^{13}C) on a Bruker spectrometer equipped with a cryoprobe. Spectral widths of 15,000 Hz in F1 and 5000 Hz in F2 were employed, with 32 scans for each of the 256 t1 increments and a relaxation delay of 1.5 s. Chemical shifts are reported in parts per million downfield from TMS as an internal standard; *J* values are given in Hz. Mass spectra were recorded on a System Applied Biosystems MDS SCIEX instrument (Q TRAP, LC/MS/MS, turbon ion spray) or on a System Applied Biosystem MDS SCIEX instrument (Q STAR elite nanospray). ESI full MS were recorded with a Thermo LTQ instrument by direct inlet; relative percentages are shown in brackets. Elemental analyses (C, H, N) were performed with a Perkin–Elmer series II 2400 analyzer or with a Perkin–Elmer CHNS/O 2400 analyse, and all synthesized compounds showed a purity of more than 95%.

3.2. Methyl (2*R*,4*S*,5*R*,6*R*)-4-(acetyloxy)-2-(2-bromoethoxy)-5-acetamido-6-[(1*R*,2*S*)-1,2,3-tris(acetyloxy)propyl]oxane-2-carboxylate (7)

To a solution of compound **6** (33 mg, 0.0626 mmol) in dry MeCN (500 μL), BrEtOH dry (44 μL, 0.626 mmol) and DAMA (7 μL, 0.0626 mmol) were added. The mixture was left under stirring for 1 h and then $BF_3{\cdot}OEt_2$ (79 μL, 0.626 mmol) was added. After 2 h satd aq $NaHCO_3$ was added to neutrality and the mixture extracted with EtOAc. The usual work up followed by flash chromatography ($CHCl_3$–EtOH 98.5:1.5) afforded compound **7** as a yellowish oil (17 mg, 47%, 33% de). ^1H NMR ($CDCl_3$): δ = 5.37 (m, 1H, 8-H), 5.31 (d, *J* = 8.7 Hz, 1H, NHAc), 5.12 (d, *J* = 9.4 Hz, 1H, 7-H), 4.87 (m, 1H, 4-H), 4.27 (dd, *J* = 2.6, 12.4 Hz, 1H, 9a-H), 4.08 (m, 4H, 5-H, 6-H, 9b-H, OCH_2a), 3.81 (s, 3H, OCH_3), 3.59 (ddd, *J* = 5.5, 7.4, 11.2 Hz, 1H, OCH_2 b), 3.44 (m, 2H, CH_2Br), 2.63 (dd, *J* = 4.7, 12.9 Hz, 1H, 3a-H). ^{13}C NMR ($CDCl_3$): δ = 171.2, 171.1, 171.0, 170.4 (s, CH_3COO), 168.2 (s, CH_3CON), 98.9 (s, 2-C), 72.1,

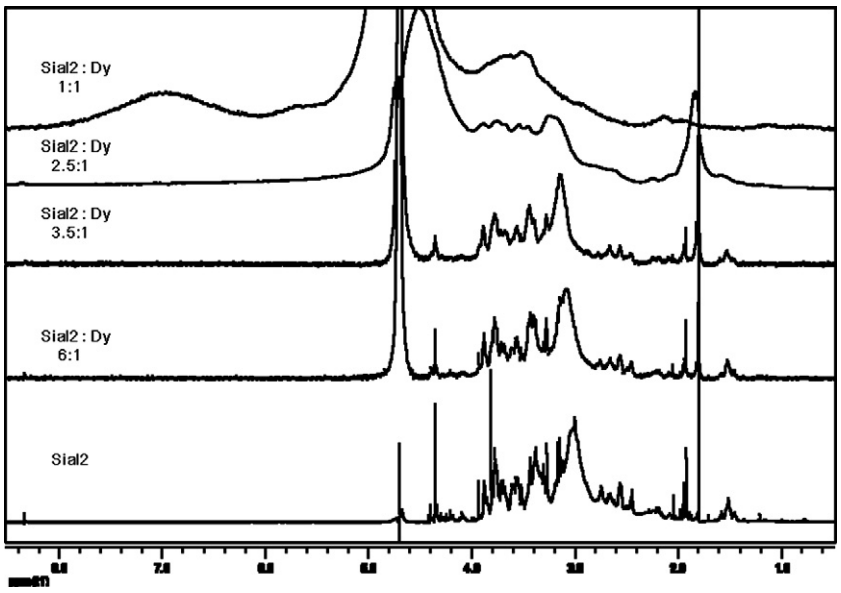

Figure 6. ^{1}H NMR spectra of **2** acquired at different molar ratios with Dy^{3+}.

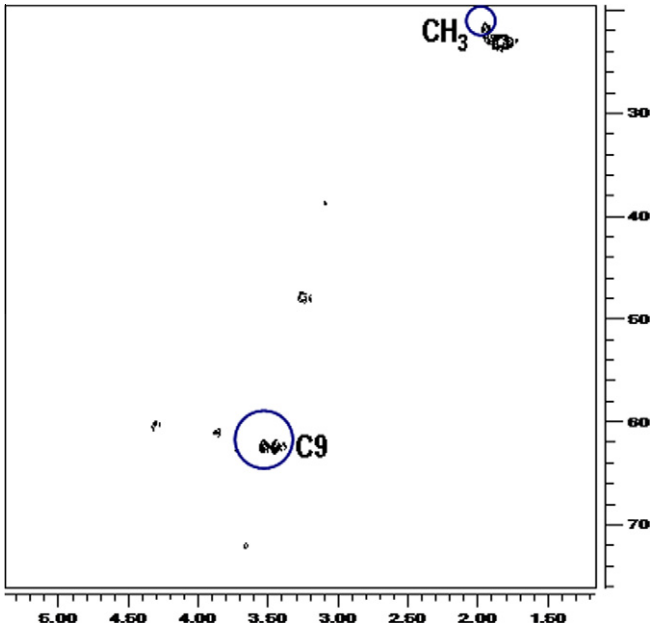

Figure 7. ^{1}H–^{13}C HSQC spectra of **2** acquired at a molar ratio 2.5:1, sialic conjugate:Dy^{3+}.

(d, 6-C), 69.2, 68.7, 67.4 (d, 4-C, 7-C, 8-C), 65.2, 62.6, (t, 9-C, 2′-C), 53.1 (q, $COOCH_3$), 49.4 (d, 5-C), 38.0, (t, 2″-C), 30.6, (t, 3-C), 21.4, (q, CH_3CON), 21.0, (q, CH_3COO). Calcd for $C_{22}H_{32}BrNO_{13}$ (598.40): C, 44.16; H, 5.39; N, 2.34. Found: C, 44.18; H, 5.38; N, 2.35.

3.3. Methyl (2*R*,4*S*,5*R*,6*R*)-4-(acetyloxy)-5-acetamido-2-[2-(1,4,7,10-tetraazacyclododecan-1-yl)ethoxy]-6-[(1*R*,2*S*)-1,2,3-tris(acetyloxy)propyl]oxane-2-carboxylate (10)

To a solution of compound **7** (50 mg, 0.083 mmol) in dry $CHCl_3$ (1 mL) cyclen (29 mg, 0.167 mmol) was added and the reaction was left stirring overnight at rt. The solvent was then evaporated under reduced pressure. The crude residue was dissolved in a small amount of water and the unreacted starting material was extracted with Et_2O. The residue obtained after water evaporation was redissolved in $CHCl_3$ to achieve the precipitation of the unreacted cyclen, that is filtered on gooch. The desired product **10** (49 mg) was obtained as yellow oil (86%). ^{1}H NMR ($CDCl_3$): $\delta = 5.33$ (m, 3H, 8-H, NH, 7-H), 4.86 (m, 1H, 4-H), 4.28 (dd, $J = 8.4$, 10.6 Hz, 1H, 9a-H), 4.05 (m, 3H, 5-H, 6-H, 9b-H), 3.81 (m, 5H, OCH_3, OCH_2), 2.86 (m, 18H, NCH_2), 2.61 (br s, 1H, 3a-H), 2.14 (s, 6H, 2 OAc), 2.02 (m, 7H, 2 OAc, 3b-H), 1.87 (s, 3H, NHAc). ^{13}C NMR ($CDCl_3$): $\delta = 171.0$, 170.8, 170.3, 170.2, 170.1 (5s, COO), 168.1 (s, CON), 98.7 (s, 2-C), 72.2, (d, 6-C), 68.9, 67.9, 67.3 (3d, 4-C, 7-C, 8-C), 62.5 (t, 9-C), 54.2 (t, 2′-C), 53.0 (d, 5-C), 51.2, 47.8, 46.4, 45.5, 45.2, 38.3, 38.0 (9t, NCH_2 cyclen, 2″-C), 49.3 (q, $COOCH_3$), 25.0 (t, 3-C), 23.2, (q, CH_3CO-N), 21.2, 21.2, 20.9, 20.8 (4q, CH_3COO). Calcd for $C_{30}H_{51}N_5O_{13}$ (689.76): C, 52.24; H, 7.45; N, 10.15. Found: C, 52.22; H, 7.44; N, 10.16.

3.4. Methyl (2*R*,4*S*,5*R*,6*R*)-5-acetamido-4-hydroxy-2-[2-(1,4,7,10-tetraazacyclododecan-1-yl)ethoxy]-6-[(1*S*,2*S*)-1,2,3-trihydroxypropyl]oxane-2-carboxylate (11)

To a solution of **10** (30 mg, 0.043 mmol) in dry MeOH (1.7 mL) catalytic Na was added. After 3 days the solvent was evaporated. Compound **11** is a yellowish oil. ^{13}C NMR ($CDCl_3$): $\delta = 184.0$ (s, COOMe), 177.6 (s, CH_3CON), 103.3 (s, 2-C), 75.4, 74.6, 71.2, 71.1 (4d, 4-C, 6-C, 7-C, 8-C), 65.3, 59.9 (2t, 9-C, 2′-C), 55.2 (d, 5-C), 47.6, 47.2, 46.0, 45.9, 45.9, 44.1 (9 t, NCH_2 cyclen, 2″-C), 26.0, (q, CH_3CON). Calcd for $C_{22}H_{43}N_5O_9$ (521.61): C, 50.66; H, 8.31; N, 13.43. Found: C, 50.65; H, 8.32; N, 13.44.

3.5. (2*R*,4*S*,5*R*,6*R*)-5-Acetamido-4-hydroxy-2-[2-(1,4,7,10-tetraazacyclododecan-1-yl)ethoxy]-6-[(1*S*,2*S*)-1,2,3-trihydroxypropyl]oxane-2-carboxylic acid (12)

To a solution of crude **11** in H_2O (1.45 mL) 116 μL of NaOH 1 M were added. After 3 days the solvent was evaporated. Compound **12** is a yellowish oil. ^{13}C NMR ($CDCl_3$): $\delta = 184.2$ (s, COOH), 171.1 (s, CH_3CON), 103.2 (s, 2-C), 77.4, 75.0, 73.2, 71.0 (4d, 4-C, 6-C, 7-C, 8-C), 65.3, 64.7 (2t, 9-C, 2′-C), 55.5 (d, 5-C), 53.6, 47.6, 47.3, 46.0, 45.4 (10t, NCH_2 cyclen, 2″-C, 3-C), 25.997 (q, CH_3CON). MS (TOF): $m/z = 508.3$ $[M+H]^+$. Calcd for $C_{21}H_{41}N_5O_9$ (507.59): C, 49.69; H, 8.14; N, 13.80. Found: C, 49.67; H, 8.15; N, 13.81.

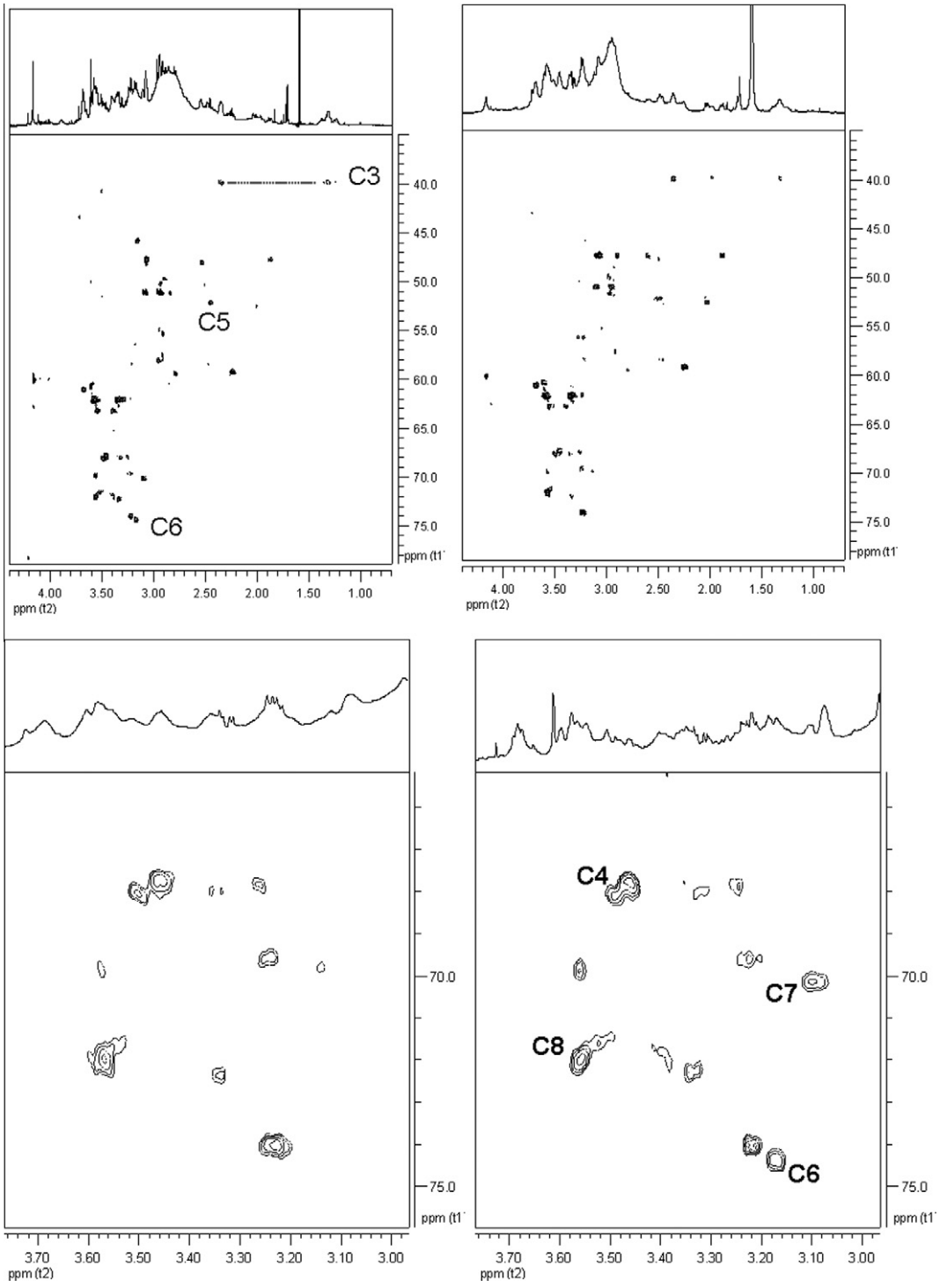

Figure 8. $^{1}H–^{13}C$ HSQC spectra of **2** and **2** complexed to Dy^{3+} at a molar ratio 3.5:1, sialic conjugate–Dy^{3+}.

3.6. (2*R*,4*S*,5*R*,6*R*)-5-Acetamido-4-hydroxy-6-[(1*S*,2*S*)-1,2,3-trihydroxypropyl]-2-{2-[4,7,10-tris(carboxymethyl)-1,4,7,10-tetraazacyclododecan-1-yl]ethoxy}oxane-2-carboxylic acid (2)

Crude **12** was dissolved in H_2O (230 μL), adjusting pH to 8 with HCl 6 N and K_2CO_3, and bromoacetic acid (5 mg, 0.035 mmol) was added. The reaction was left stirring at room temperature for 2 days, filtered on gooch and the solvent was then evaporated under reduced pressure giving the desired crude product **2**. MS (TOF): m/z = 680.3 $[M-H]^-$. Calcd for $C_{27}H_{47}N_5O_{15}$ (681.70): C, 47.57; H, 6.95; N, 10.27. Found: C, 47.59; H, 6.96; N, 10.28.

3.7. [Gd{(2*R*,4*S*,5*R*,6*R*)-5-Acetamido-4-hydroxy-6-[(1*S*,2*S*)-1,2,3-trihydroxypropyl]-2-{2-[4,7,10-tris(carboxymethyl)-1,4,7,10-tetraazacyclododecan-1-yl]ethoxy}oxane-2-carboxylic acid}] (4)

To a solution of crude **2** in H_2O (600 μL) $GdCl_3·6H_2O$ (4 mg, 0.0096 mmol) was added and pH adjusted to 5.5. The reaction was left stirring at room temperature for 3 days monitoring by MS. To precipitate the metal in excess pH was brought up to 9 with NaOH 0.1 M and the mixture was then centrifuged. After adjusting pH to 7 the solution was freeze-dried giving crude **4** as a white pow-

der. MS (TOF): m/z = 835.2 $[M]^-$. Calcd for $C_{27}H_{43}GdN_5O_{15}$ (834.92): C, 38.84; H, 5.19; N, 8.39. Found: C, 38.82; H, 5.18; N, 8.38.

3.8. Computational methods

$[Gd(Sial)]^-$ geometry was built from the crystallographic structure of [Gd(HP-DO3A)].[32] In the crystallographic cell of [Gd(HP-DO3A)], two diastereoisomeric conformations, namely $\Lambda(\delta\delta\delta\delta)$ and $\Lambda(\lambda\lambda\lambda\lambda)$, are present and differ only in the configuration of the cyclen: these two conformations are labelled as (A+) and (A−), respectively. Their geometries were modified in order to obtain the two other possible diastereoisomeric conformations, namely the $\Delta(\delta\delta\delta\delta)$ and $\Delta(\lambda\lambda\lambda\lambda)$ ones, presenting opposite orientations of the arms, labelled as (B+) and (B−). Then, the sialic moiety was connected obtaining the four $[Gd(Sial)]^-$ diastereoisomeric conformations: these were optimized in vacuo at the MM level by the appropriate force fields[44] in the Sybyl software package.[45] On the basis of their relative energies, the (A+) conformation was selected for further analysis.

3.9. Molecular dynamics simulations

Three starting conformations, differing in the orientation of the sialic moiety, were considered for simulations. Each complex was hydrated in a periodic cubic box, approximately 42 Å long per edge, containing about 2500 Extended Simple Point Charge (SPC/E) water molecules.[46] No counter-ion was added to the $[Gd(Sial)]^-$ system. The simulations were performed by the GROMACS (version 3.3) package,[47] using the previously developed force fields[31] (Table 2S).

Non-bonding interactions were evaluated using a twin range cut-off. The pair list within the shorter-range cut-off (9.0 Å) was evaluated at each step, whereas the pair list within the longer cut-off (14.0 Å) was updated every five steps. To correct for the neglect of electrostatic interactions beyond the 14.0 Å cut-off, a reaction field (RF) correction[48] with ε_{RF} = 78.0 was used. A preliminary steepest descendent optimization of the solvated complexes was done. Each system was then submitted to a MD run. To maintain constant temperature and pressure, the Berendsen algorithm[49] was applied. The complex and the solvent were independently coupled to a temperature bath (298 K) with a coupling time of 0.1 ps. The pressure was held at 1 bar, with a coupling time of 0.5 ps. The isothermal compressibility was 4.5×10^{-5} bar^{-1}. Bond lengths within the complexes involving hydrogen atoms were constrained using the LINCS algorithm;[50] the bond lengths and angle in the water molecules were constrained using the SETTLE algorithm.[51] Time step was 2.0 fs; simulation time was 20.0 ns for each run; equilibration time was 0.1 ns. Table 3S shows the relevant simulation parameters. Coordinates were stored every 0.5 ps. Atomic charges used in the MD simulations were calculated by fitting the in vacuo HF/6-311G** molecular electrostatic potential (MEP) by means of the Merz–Kollman method.[52] The charges of atoms with the same MM atom-type and similar chemical environment were then averaged using RESP software.[53] The list of the atomic charges is reported in Table 4S of the Supplementary data.

3.10. Ab initio calculations

Ab initio calculations on $[Gd(Sial)(H_2O)]^-$ use the quasi-relativistic effective core potential (ECP) of Dolg et al.,[54] and the related [5s4p3d]-GTO valence basis sets for the gadolinium ion. This ECP includes 46+4f^n electrons in the core, leaving the outermost 11 electrons to be treated explicitly. Following the previously adopted computational procedure,[44,55] geometry optimizations were performed at the restricted HF level using the 3-21G basis set for the ligand atoms. On the optimized structures, DFT single point energy calculations were performed with the PBE1PBE functional,[56] using the 6-311G** basis sets for the ligand.[57] Solvent effects were evaluated by the C-PCM variant[58] of GAUSSIAN 03.[59] In line with the united atom topological model (UATM),[60] the solute cavity is built as an envelope of spheres centred on atoms or atomic groups with appropriate radii. For the gadolinium(III) ion, the previously parameterized radius[61] was used, neglecting the gadolinium dispersion and repulsion parameters due to their negligible influence in aqueous solution. All the UATM radii were scaled by a factor of 1.2 in the calculation of electrostatic contributions, while unscaled values were used to calculate other contributions. To avoid convergence problems during geometry optimization, the non-electrostatic contributions to the energy and energy gradient, viz., cavitation, dispersion, and repulsion contributions, were omitted. Due to the slow convergence the optimization was, in some cases, stopped when the convergence parameters were less than twice the default values. For this reason frequency analysis was not performed to characterize the stationary points; thus, the final geometries correspond to stable conformations for the chosen minimization algorithm, rather than true minima. As PCM results have free energies status, total free energy in solution is labelled as G^{tot}, in vacuo total energy as E°, and solvation free energy as ΔG^{sol}. Total free energies in solution obtained from single point calculations at optimized geometries in solution include both the electrostatic and non-electrostatic contributions of all atoms, the exception being the dispersion and repulsion contributions of gadolinium, which are omitted. All the calculations were done using the GAUSSIAN 03 package.[59]

4. Conclusions

We proposed here the synthesis of a DOTA-like sialic acid conjugate that, upon complexation with suitable paramagnetic metals, can be used both for MRI and PRE applications. Both theoretical and experimental characterization of this system suggest that the sialic moiety can prevent the coordination of the water molecule to the paramagnetic ion; as a result, the complex should exist in a low-relaxivity (MRI 'inactive') state prone to be switched to a MRI 'active' state upon cleavage of the sugar moiety by the sialidase. The conjugate, however, exists in solution in different conformations (as deduced form line broadening in the ^1H NMR spectrum), thus limiting the efficiency of the system.

Acknowledgements

We gratefully acknowledge financial supports from the University of Milano-Bicocca (FAR2008) and computational facilities from CILEA (Consorzio Interuniversitario Lomabardo per l'Elaborazione Automatica), Programma Operativo Regione Lombardia Ob. 3 Fondo Sociale Europeo 2000–2006, Sovvenzione Globale Progetto Ingenio A0001127/2007 and Consorzio Interuniversitario Nazionale 'Metodologie e Processi Innovativi di Sintesi' (C.I.N.M.P.I.S.).

Supplementary data

Supplementary data (computational details: atomic charges, parameter set, simulation parameters) associated with this article can be found, in the online version, at http://dx.doi.org/10.1016/j.carres.2012.03.002.

References

1. (a) Schauer, R. *Zoology* **2004**, *107*, 49–64; (b) Corfield, A. P.; Schauer, R. In Schauer, R., Ed.; Sialic Acids, Chemistry, Metabolism and Function in Cell Biology Monograph; Springer: New York, 1982; Vol. 2, p 5.

2. Varki, A.; Cummings, R.; Esko, J.; Freeze, H.; Stanley, P.; Bertozzi, C.; Hart, G.; Etzler, M. In *Essentials of Glycobiology*, 2nd ed.; Cold Spring Harbor Laboratory Press: New York, 2008.
3. Ahmad, F.; McPhile, P. *Int. J. Biochem.* **1980**, *11*, 91–96.
4. Kemp, R. B. *J. Cell Sci.* **1970**, *6*, 751–766.
5. Severi, E.; Hood, D. W.; Thomas, G. H. *Microbiology* **2007**, *153*, 2817–2822.
6. Karlsson, K.-A. *Curr. Opin. Struct. Biol.* **1995**, *5*, 622–635.
7. (a) Ito, Y.; Gaudino, J. J.; Paulson, J. C. *Pure Appl. Chem.* **1993**, *65*, 753–762; (b) Paulson, J. C. In *The Receptors*; Conn, M., Ed.; Academic Press: New York, 1985; Vol. 2, p 131; (c) Olofsson, S.; Bergstrom, T. *Ann. Med.* **2005**, *37*, 154–172.
8. (a) Springer, T. A.; Larsky, L. A. *Nature* **1991**, *349*, 196–197; (b) Paulson, J. C. In *Adhesion: Its Role in Inflammatory Diseases*; Harlan, J. M., Liu, D. Y., Eds.; WH Freeman: New York, 1992; p 19; (c) Chabre, Y. M.; Roy, R. In *The Sugar Code. Fundamentals of Glycosciences*; Gabius, H.-J., Ed.; Wiley-VCH: Weinheim, 2009.
9. (a) Yogeeswaran, G.; Salk, P. *Science* **1981**, *212*, 1514–1516; (b) Fogel, M.; Altevogt, P.; Schirrmacher, V. *J. Exp. Med.* **1983**, *157*, 371–376; (c) Collard, J. G.; Schijven, J. F.; Bikker, A.; La Riviere, G.; Bolscher, J. G. M.; Roos, E. *Cancer Res.* **1986**, *46*, 3521–3527; (d) Dennis, J. W.; Lafarté, S.; Waghorne, C.; Breitman, M. L.; Kerbel, R. S. *Science* **1987**, *236*, 582–585; (e) Passaniti, A.; Hart, G. W. *J. Biol. Chem.* **1988**, *263*, 7591–7603.
10. (a) Kim, Y. J.; Varki, A. *Glycoconjugate J.* **1997**, *14*, 569–576; (b) Hakomori, S. *Cancer Res.* **1996**, *56*, 5309–5318; (c) Hakomori, S.; Yamamura, S.; Handa, A. K. *Ann. N.Y. Acad. Sci.* **1998**, *845*, 1–10.
11. Miyagi, T.; Wada, T.; Yamaguchi, K.; Hata, K. *Glycoconjugate J.* **2003**, *20*, 189–198.
12. Hakomori, S. *Proc. Natl. Acad. Sci. U.S.A.* **2002**, *99*, 10231–10233.
13. Kakugawa, Y.; Wada, T.; Yamaguchi, K.; Yamanami, H.; Ouchi, K.; Sato, I.; Miyagi, T. *Proc. Natl. Acad. Sci. U.S.A.* **2002**, *99*, 10718–10723.
14. (a) Cheng, H.; Markley, J. L. *Ann. Rev. Biophys. Biomol. Struct.* **1995**, *24*, 209–237; (b) Bertini, I.; Luchinat, C.; Licciolini, M. *Methods Enzymol.* **2001**, *339*, 314–340; (c) Ubbink, M.; Worral, J. A. R.; Canters, G. W.; Groenen, E. J. J.; Huber, M. *Ann. Rev. Biophys. Biomol. Struct.* **2002**, *31*, 393–422; (d) Sharp, R. R. *Nucl. Magn. Reson.* **2005**, *34*, 553–596.
15. See for example: (a) Meade, T. J. *Acc. Chem. Res.* **2009**, *42*, 821; (b) Yoo, B.; Pagel, M. D. *Front. Biosci.* **2008**, *13*, 1733–1752.
16. (a) Caravan, P.; Ellison, J. J.; McMurry, T. J.; Lauffer, R. B. *Chem. Rev.* **1999**, *99*, 2293–2352; (b) Merbach, A. E.; Toth, E. *The Chemistry of Contrast Agents in Medical Magnetic Resonance Imaging*; John Wiley and Sons Ltd: West Sussex, 2001.
17. (a) Woods, M.; Kovacs, Z.; Sherry, A. D. *J. Supramol. Chem.* **2002**, *2*, 1–15; (b) Aime, S.; Geninatti Crich, S.; Gianolio, E.; Giovenzana, G. B.; Tei, L.; Terreno, E. *Coord. Chem. Rev.* **2006**, *250*, 1562–1579.
18. Louie, A. Y.; Huber, M. M.; Ahrens, E. T.; Rothbacher, U.; Moats, R.; Jacobs, R. E.; Fraser, S. E.; Meade, T. J. *Nat. Biotechnol.* **2000**, *18*, 321–325.
19. Clore, G. M.; Tang, C.; Iwahara, J. *Curr. Opin. Struct. Biol.* **2007**, *17*, 603–616. and references cited therein.
20. Bloembergen, N.; Morgan, L. O. *J. Chem. Phys.* **1961**, *34*, 842–850.
21. (a) Mahoney, N. M.; Rastogi, V. K.; Cahill, S. M.; Girvin, M. E.; Almo, S. C. *J. Am. Chem. Soc.* **2000**, *122*, 7851–7852; (b) Mal, T. K.; Ikura, M.; Kay, L. E. *J. Am. Chem. Soc.* **2002**, *124*, 14002–14003; (c) Gross, J. D.; Moerke, N. J.; Van deer Haar, R.; Lugovsky, A. A.; Sachs, A. B.; McCarthy, J. E.; Wagner, G. *Cell* **2003**, *115*, 739–750; (d) Card, P. B.; Erbel, P. J. A.; Gardner, K. H. *J. Mol. Biol.* **2005**, *353*, 664–677.
22. (a) Johnson, P. E.; Brun, E.; MacKenzie, L. F.; Withers, S. G.; McIntosh, L. P. *J. Mol. Biol.* **1999**, *287*, 609–625; (b) Jain, N. U.; Venot, K.; Umemoto, H.; Leffler, H.; Prestegard, J. H. *Protein Sci.* **2001**, *10*, 2393–2400; (c) Macnaughtan, M. A.; Kamar, M.; Alvarez-Manilla, G.; Venot, A.; Glushka, J.; Pierce, J. M.; Prestegard, J. H. *J. Mol. Biol.* **2007**, *366*, 1266–1281.
23. (a) Lemieux, G. A.; Yarema, K. J.; Jacobs, C. L.; Bertozzi, C. R. *J. Am. Chem. Soc.* **1999**, *121*, 4278–4279; (b) Frullano, L.; Rohovec, J.; Aime, S.; Maschmeyer, T.; Prata, M. I.; Pedroso de Lima, J. J.; Geraldes, C. F. G. C.; Peters, J. A. *Chem. Eur. J.* **2004**, *10*, 5205–5217; (c) Shelke, S. V.; Cutting, B.; Jiang, X.; Koliwer-Brandl, H.; Strasser, D. S.; Schwardt, O.; Kelm, S.; Ernst, B. *Angew. Chem., Int. Ed.* **2010**, *49*, 5721–5725.
24. Cipolla, L.; Gregori, M.; So, P.-W. *Curr. Med. Chem.* **2011**, *18*, 1002–1018.
25. Duimstra, J. A.; Femia, F. J.; Meade, T. J. *J. Am. Chem. Soc.* **2005**, *127*, 12847–12855.
26. (a) Urbanczyk-Pearson, L. M.; Femia, F. J.; Smith, J.; Parigi, G.; Duimstra, J. A.; Eckermann, A. L.; Luchinat, C.; Meade, T. J. *Inorg. Chem.* **2008**, *47*, 56–68; (b) Urbanczyk-Pearson, L. M.; Meade, T. J. *Nat. Protocols* **2008**, *3*, 341–350.
27. Briggsg, J.; Frosti, H.; Hart, A.; Moss, G. P.; Stanifor, M. L. *Chem. Commun.* **1970**, 749–750.
28. (a) Bernardi, A.; Arosio, D.; Potenza, D.; Sánchez-Medina, I.; Mari, S.; Cañada, F. J.; Jiménez-Barbero, J. *Chem. Eur. J.* **2004**, *10*, 4395–4406; (b) Politi, M.; Alvaro-Blanco, J.; Groves, P.; Prieto, A.; Leal, J. A.; Cañada, F. J.; Jiménez-Barbero, J. *Eur. J. Org. Chem.* **2006**, 2067–2073; (c) Ernst, B.; Magnani, J. L. *Nat. Rev. Drug Disc.* **2009**, *8*, 661–677.
29. Tomasi, J.; Persico, M. *Chem. Rev.* **1994**, *94*, 2027–2094.
30. Amovilli, C.; Barone, V.; Cammi, R.; Cances, E.; Cossi, M.; Mennucci, B.; Pomelli, C. S.; Tomasi, J. *Adv. Quantum Chem.* **1998**, *32*, 227–261.
31. Cosentino, U.; Pitea, D.; Moro, G.; Saracino, G. A. A.; Villa, A. *PCCP* **2009**, *11*, 3943–3950.
32. Kumar, K.; Chang, C. A.; Francesconi, L. C.; Dischino, D. D.; Malley, M. F.; Gougoutas, J. Z.; Tweedle, M. F. *Inorg. Chem.* **1994**, *33*, 3567–3575.
33. Kononov, L. O.; Magnusson, G. *Acta Chem. Scand.* **1998**, *52*, 141–144.
34. (a) Ress, D. K.; Linhardt, R. J. *Curr. Org. Synth.* **2004**, *1*, 31–46; (b) Boons, G.-J.; Demchenko, A. V. *Chem. Rev.* **2000**, *100*, 4539–4565.
35. Koenigs, W.; Knoor, E. *Chem. Ber.* **1901**, *34*, 957–981.
36. De Smet, L. C. P. M.; Pukin, A. V.; Stork, G. A.; De Vos, C. H. R.; Visser, G. M.; Zuilhof, H.; Sudhölte, E. J. R. *Carbohydr. Res.* **2004**, *339*, 2599–2605.
37. Lu, K. C.; Tseng, S. Y.; Lin, C. C. *Carbohydr. Res.* **2002**, *337*, 755–760.
38. (a) Pougny, J.; Sinaÿ, P. *Tetrahedron Lett.* **1976**, *45*, 4073–4076; (b) Braccini, I.; Derouet, C.; Esnault, J.; Herve du Penhoat, C.; Mallet, J.-M.; Michon, V.; Sinaÿ, P. *Carbohydr. Res.* **1993**, *246*, 23–41; (c) Schmidt, R. R.; Castro-Palomino, J. C.; Retz, O. *Pure Appl. Chem.* **1999**, *71*, 729–744.
39. Kononov, L. O.; Malysheva, N. N.; Orlova, A. V. *Eur. J. Org. Chem.* **2009**, 611–616.
40. (a) Guillaume, D.; Marshall, G. R. *Synth. Commun.* **1998**, *28*, 2903–2906; (b) Maillet, M.; Kwok, C. S.; Noujaim, A. A.; Snieckus, V. *Tetrahedron Lett.* **1998**, *39*, 2659–2662; (c) Bender, J. A.; Meanwell, N. A.; Wang, T. *Tetrahedron* **2002**, *58*, 3111–3128.
41. Zèmplen, G. *Chem. Ber.* **1926**, *59*, 1254–1266.
42. Rencurosi, A.; Poletti, L.; Guerrini, M.; Russo, G.; Lay, L. *Carbohydr. Res.* **2002**, *337*, 473–483.
43. Häussinger, D.; Huang, J.-R.; Grzesiek, S. *J. Am. Chem. Soc.* **2009**, *131*, 14761–14767.
44. (a) Cosentino, U.; Moro, G.; Pitea, D.; Villa, A.; Fantucci, P. C.; Maiocchi, A.; Uggeri, F. *J. Phys. Chem. A* **1998**, *102*, 4606–4614; (b) Villa, A.; Cosentino, U.; Pitea, D.; Moro, G.; Maiocchi, A. *J. Phys. Chem. A* **2000**, *104*, 3421–3429.
45. Tripos Inc.: 1699 S. Hanley Road, St. Louis, MO, 63144, SYBYL 7.2, 2006.
46. Berendsen, H. J. C.; Grigera, J. R.; Straatsma, T. P. *J. Phys. Chem.* **1987**, *91*, 6269–6271.
47. (a) Berendsen, H. J. C.; van der Spoel, D.; van Drunen, R. *Comput. Phys. Commun.* **1995**, *91*, 43–56; (b) Lindahl, E.; Hess, B.; van der Spoel, D. *J. Mol. Model.* **2001**, *7*, 306–317.
48. Tironi, I. G.; Sperb, R.; Smith, P. E.; van Gunsteren, W. F. *J. Chem. Phys.* **1995**, *102*, 5451–5459.
49. Berendsen, H. J. C.; Postma, J. P. M.; van Gunsteren, W. F.; Di Nola, A.; Haak, J. R. *J. Chem. Phys.* **1984**, *81*. 3684–360.
50. Hess, B.; Bekker, H.; Berendsen, H. J. C.; Fraaije, J. G. E. M. *J. Comput. Chem.* **1997**, *18*, 1463–1472.
51. Miyamoto, S.; Kollman, P. A. *J. Comput. Chem.* **1992**, *13*, 952–962.
52. Besler, B. H.; Merz, K. M.; Kollman, P. A. *J. Comput. Chem.* **1990**, *11*, 431–439.
53. Bayly, C. I.; Cieplak, P.; Cornell, W. D.; Kollman, P. A. *J. Phys. Chem.* **1993**, *97*, 10269–10280.
54. Dolg, M.; Stoll, H.; Savin, A.; Preuss, H. *Theor. Chim. Acta* **1989**, *75*, 173–194.
55. Cosentino, U.; Villa, A.; Pitea, D.; Moro, G.; Barone, V.; Maiocchi, A. *J. Am. Chem. Soc.* **2002**, *124*, 4901–4909.
56. Adamo, C.; Barone, V. *J. Chem. Phys.* **2002**, *116*, 5933–5940.
57. Description of the basis sets and explanation of standard levels of theory can be found in: Foresman, J. B.; Frisch, A. E. *Exploring Chemistry with Electronic Structure Methods*, 2nd ed.; Gaussian Inc.: Pittsburgh, PA, 1996.
58. (a) Barone, V.; Cossi, M. *J. Phys. Chem. A* **1998**, *102*, 1995–2001; (b) Cossi, M.; Rega, N.; Scalmani, G.; Barone, V. *J. Comput. Chem.* **2003**, *24*, 669–681.
59. Frisch, M. J.; Trucks, G. W.; Schlegel, H. B.; Scuseria, G. E.; Robb, M. A.; Cheeseman, J. R.; Montgomery, J. A., Jr.; Vreven, T.; Kudin, K. N.; Burant, J. C.; Millam, J. M.; Iyengar, S. S.; Tomasi, J.; Barone, V.; Mennucci, B.; Cossi, M.; Scalmani, G.; Rega, N.; Petersson, G. A.; Nakatsuji, H.; Hada, M.; Ehara, M.; Toyota, K.; Fukuda, R.; Hasegawa, J.; Ishida, M.; Nakajima, T.; Honda, Y.; Kitao, O.; Nakai, H.; Klene, M.; Li, X.; Knox, J. E.; Hratchian, H. P.; Cross, J. B.; Bakken, V.; Adamo, C.; Jaramillo, J.; Gomperts, R.; Stratmann, R. E.; Yazyev, O.; Austin, A. J.; Cammi, R.; Pomelli, C.; Ochterski, J. W.; Ayala, P. Y.; Morokuma, K.; Voth, G. A.; Salvador, P.; Dannenberg, J. J.; Zakrzewski, V. G.; Dapprich, S.; Daniels, A. D.; Strain, M. C.; Farkas, O.; Malick, D. K.; Rabuck, A. D.; Raghavachari, K.; Foresman, J. B.; Ortiz, J. V.; Cui, Q.; Baboul, A. G.; Clifford, S.; Cioslowski, J.; Stefanov, B. B.; Liu, G.; Liashenko, A.; Piskorz, P.; Komaromi, I.; Martin, R. L.; Fox, D. J.; Keith, T.; Al-Laham, M. A.; Peng, C. Y.; Nanayakkara, A.; Challacombe, M.; Gill, P. M. W.; Johnson, B.; Chen, W.; Wong, M. W.; Gonzalez, C.; Pople, J. A. GAUSSIAN *03, Revision C.02*; Gaussian, Inc.: Wallingford CT, 2004.
60. Barone, V.; Cossi, M.; Tomasi, J. *J. Chem. Phys.* **1997**, *107*, 3210–3221.
61. Cosentino, U.; Villa, A.; Pitea, D.; Moro, G.; Barone, V. *J. Phys. Chem. B* **2000**, *104*, 8001–8007.